



# Oriented 2.0.0 Cu<sub>2</sub>O nanoplatelets supported on few-layers graphene as efficient visible light photocatalyst for overall water splitting

Diego Mateo, Iván Esteve-Adell, Josep Albero, Ana Primo, Hermenegildo García\*

*Instituto de Tecnología Química, Universitat Politècnica de València-Consejo Superior de Investigaciones Científicas, Avenida de los Naranjos s/n, 46022 Valencia, Spain*

## ARTICLE INFO

### Article history:

Received 3 May 2016

Received in revised form 9 August 2016

Accepted 16 August 2016

Available online 31 August 2016

### Keywords:

Preferential orientation

Photocatalysis

Graphene

Nanoplatelet

Water splitting

## ABSTRACT

Cu<sub>2</sub>O nanoplatelets with preferential 2.0.0 facet orientation supported on few layers graphene were prepared as films in a single step by pyrolysis at 900 °C under inert atmosphere of Cu<sup>2+</sup>-chitosan precursor.

Cu<sub>2</sub>O/fl-G films exhibit a photocatalytic activity for overall water splitting of 19.5 mmol/g<sub>Cu+G</sub> h. This value is about 4 orders of magnitude higher than the photocatalytic activity measured for unoriented Cu<sub>2</sub>O nanoparticles on few-layers graphene or than commercial Cu<sub>2</sub>O nanoparticles and about three orders of magnitude higher than the activity reported in the literature for Cu<sub>2</sub>O nanoparticles. In addition Cu<sub>2</sub>O nanoparticles on few-layers graphene retain about 50% of its photocatalytic activity after 6 days of continuous irradiation. It is proposed that this activity and stability arises from the combination of features derived from the pyrolysis preparation procedure including strong Cu<sub>2</sub>O-graphene grafting, the role of graphene as cocatalyst and preferential 2.0.0 facet orientation.

© 2016 Elsevier B.V. All rights reserved.

## 1. Introduction

Supported metal nanoparticles (MNPs) on high surface area solids have been extensively used in heterogeneous catalysis to promote a large variety of organic reactions [1,2] including reductions [3], oxidations [4] and cross-couplings [5]. More recently, supported MNPs are finding increasing application for energy production and storage [6,7].

There are ample precedents showing that the catalytic activity of supported MNPs can be strongly influenced by the support [8,9]. In this regard, graphene (G), which constitutes the physical limit of 2D materials, is attracting much interest not only as metal-free catalyst, but also as support of MNPs [10–12]. The interest in the use of G as support derives from its unique properties, including large surface area, high adsorption capacity, possibility to form films coating arbitrary substrates and, importantly, the strong MNP-G interaction that may arise from the overlap of the extended  $\pi$  orbital of G with the d orbitals of transition metals [12–15].

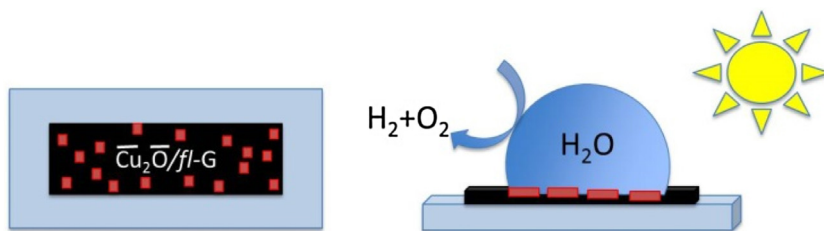
More relevant to our work, MNPs supported on G have been reported to exhibit photocatalytic activity [16,17], including H<sub>2</sub> evolution from water containing sacrificial electron donors. Supported noble MNPs (Pt, Au, Ag etc.) have been widely reported in the

literature as co-catalysts to increase the efficiency of photocatalytic H<sub>2</sub> generation under UV or/and visible light irradiation [18–20]. However, the use of critical metals can be a strong limitation for the wide applicability of these photocatalysts for H<sub>2</sub> generation and it is much more convenient the use of Earth-abundant and low-cost metals, such as Cu. In this regard, Cu<sub>2</sub>O is a relatively non-toxic substance that exists abundantly in Nature as cuprite. Cu<sub>2</sub>O is a semiconducting oxide with 2.0 eV band gap capable to promote photocatalytic water splitting upon visible light irradiation [21]. Domen and co-workers reported the photocatalytic overall decomposition of water into H<sub>2</sub> and O<sub>2</sub> on Cu<sub>2</sub>O particles of 300–500 nm size upon irradiation with visible light in the absence of any sacrificial electron donor at rates of approximately 2  $\mu$ mol/g·h without observing decrease in the H<sub>2</sub> evolution for more than 1900 h [22]. The photocatalytic activity of Cu<sub>2</sub>O to promote the overall water splitting has been later by confirmed other research groups [23–25] and supported by first-principles calculations that show that the conduction and valence bands of most stable facets of Cu<sub>2</sub>O should have enough energy to promote overall water splitting and CO<sub>2</sub> reduction [26].

In the area of catalysis by MNPs, theoretical as well as scattered experimental data have shown that different crystallographic planes may exhibit different specific activity [27,28]. Accordingly, there has been an increasing interest in controlling the preferential facets of MNPs exposed to the reaction to determine the influence of this parameter on the (photo)catalytic activity of MNPs. Specif-

\* Corresponding author.

E-mail address: [hgarcia@qim.upv.es](mailto:hgarcia@qim.upv.es) (H. García).



**Scheme 1.** Pictorial representation of a frontal view of films of oriented Cu<sub>2</sub>O nanoplatelets (small orange squares) supported on few-layers G (black large rectangle) deposited on a quartz substrate (light blue rectangle) and the process of photocatalytic H<sub>2</sub> and O<sub>2</sub> evolution from pure, liquid H<sub>2</sub>O without stirring using the Cu<sub>2</sub>O/fl-G film on quartz (presented in a lateral view) illuminated with UV-vis light. (For interpretation of the references to color in this scheme legend, the reader is referred to the web version of this article.)

ically in the case of the photocatalytic overall water splitting into H<sub>2</sub> and O<sub>2</sub>, Lee et al. found that the morphology of Cu<sub>2</sub>O NPs influences their activity and stability for H<sub>2</sub> production from water upon visible light irradiation [24]. In that work, cubes, octahedra and rhombic dodecahedra, exhibiting, respectively, preferential (1.0.0), (1.1.1) and (1.1.0) facets, presented a H<sub>2</sub> production of 0, 0.5 and 1.6 μmol/g h, for each type of crystallite. However, a fast degradation of the photocatalytic activity was found due to photocorrosion of Cu<sub>2</sub>O to CuO during the H<sub>2</sub> production, resulting in unacceptable poor stability. The influence of the crystallographic facets of Cu<sub>2</sub>O on the band energies and stability has also been addressed using DFT calculations [26]. Thus, it would be important to find a way to prepare oriented Cu<sub>2</sub>O nanoparticles stable under photocatalytic H<sub>2</sub> generation.

In the present manuscript, we have prepared by a novel one-step pyrolysis procedure [29] oriented Cu<sub>2</sub>O nanoplatelets having preferential (2.0.0) facet orientation strongly interacting with few-layers G (Cu<sub>2</sub>O/fl-G, Cu<sub>2</sub>O meaning 2.0.0 oriented, fl meaning few layers) exhibit much higher photocatalytic activity for overall H<sub>2</sub>O splitting in the absence of any sacrificial electron agent than those photocatalysts of Cu<sub>2</sub>O previously reported or than analogous materials based on unoriented Cu<sub>2</sub>O supported on fl-G (Cu<sub>2</sub>O-fl-G). A remarkable positive influence of (2.0.0) facet orientation, strong metal oxide-support interaction and electron mobility on G on the photocatalytic activity has been established by comparing the H<sub>2</sub> evolution of oriented and unoriented Cu<sub>2</sub>O NPs adsorbed on few layers G (Cu<sub>2</sub>O/fl-G) under visible light irradiation (Scheme 1). As consequence of these favorable features the Cu<sub>2</sub>O/fl-G photocatalyst produced at least three magnitude orders higher H<sub>2</sub> production (in the range of mmol/g<sub>Cu</sub>·h rather than μmol/g<sub>Cu</sub> h) respect the unoriented Cu<sub>2</sub>O/fl-G film or suspended Cu<sub>2</sub>O NPs. In addition, in spite of the small average particle size of oriented Cu<sub>2</sub>O nanoplatelets compared to those in the micrometric length scale reported in the literature [22], it was found that these Cu<sub>2</sub>O/fl-G samples can operate for six days without appreciable change in the particle size distribution and retaining a considerable percentage of its photocatalytic activity, thus proving the remarkable stability under photocatalytic conditions.

## 2. Experimental

### 2.1. Synthesis of catalyst

Preparation of Cu<sub>2</sub>O/fl-G. Cu<sub>2</sub>O/fl-G films were prepared as reported before [29]. In brief, chitosan (0.5 g) from Aldrich (low molecular weight) was dissolved in a copper (II) nitrate aqueous solution (18 mg of Cu(NO<sub>3</sub>)<sub>2</sub>·2H<sub>2</sub>O in 25 ml of water) by addition of 0.23 g of acetic acid. To remove insoluble impurities typically present in commercial chitosan, the solution was filtered through a syringe having a membrane filter of 0.45 μm diameter pore

size. Films of chitosan containing Cu(NO<sub>3</sub>)<sub>2</sub> coating quartz plates (2 × 2 cm<sup>2</sup>) were obtained by casting 300 μl of filtered solution at 6000 r.p.m. in 1 min. Conversion of chitosan into graphene and formation of Cu metal nanoparticles was performed by pyrolysis under argon atmosphere in a tubular oven heating at a rate of 5 °C min<sup>-1</sup> up to 900 °C with a hold time of 2 h. The sample was, then, cooled at room temperature under argon. The resulting sample immediately after the pyrolysis consisted in metallic Cu nanoplatelets grafted on G that undergo spontaneous Cu oxidation to Cu<sub>2</sub>O/fl-G. upon exposure to the ambient. The samples used in the present study were aged for at least two days, before being used as photocatalysts.

#### 2.1.1. Preparation of Cu<sub>2</sub>O/fl-G

A suspension of few-layers graphene in ethylene glycol (40 ml) was obtained by sonication at 700 W for 1 h of a carbon residue (100 mg) obtained from the pyrolysis of alginic acid sodium salt from brown algae (Aldrich) until a well dispersed fl-G ink was observed. CuCl<sub>2</sub> (1.06 mg for the preparation of the sample at 0.1 wt% Cu<sub>2</sub>O) was added to the reaction mixture and Cu metal reduction was then performed at 120 °C for 24 h under continuous stirring. The Cu/fl-G samples were finally recovered by filtration and washed exhaustively with water and with acetone. The resulting material was dried in a vacuum desiccator at 110 °C to remove the remaining water. Spontaneous oxidation of Cu/fl-G by exposure to the ambient for longer than two days renders the control sample Cu<sub>2</sub>O/fl-G, having unoriented Cu<sub>2</sub>O NPs. Preparation of films of unoriented Cu<sub>2</sub>O on quartz for XRD measurements was performed by casting a few drops of a suspension of Cu<sub>2</sub>O/fl-G on water freshly prepared by ultrasonication on a clean quartz slide.

#### 2.1.2. Ethanolic suspension of Cu<sub>2</sub>O

This sample was purchased from Aldrich (1.5% (w/v)). The amount of copper present in the samples was determined by inductively coupled plasma-optical emission spectrometry (ICP-OES) by immersing the plates into aqua regia at room temperature for 3 h and analyzing the Cu content of the resulting solution.

### 2.2. Characterization of catalysts

Powder XRD patterns were recorded on a Shimadzu XRD-7000 diffractometer using Cu K $\alpha$  radiation ( $\lambda = 1.5418 \text{ \AA}$ , 40 kV, 40 mA) at a scanning speed of 1° per min in the 10–80° 2θ range.

Raman spectrum was collected with a Horiba Jobin Yvon-Labram HR UV-vis-NIR (200–1600 nm) Raman Microscope Spectrometer, using a laser with the wavelength of 632 nm. The spectrum was collected from 10 scans at a resolution of 2 cm<sup>-1</sup>.

Scanning electron microscopy (SEM) images were recorded with a Zeiss Ultra 55 field emission scanning electron microscope (FESEM) apparatus. The crystal phase of the Cu NPs was determined by FESEM using an electron backscatter diffraction detector inside the chamber and transmission electron microscopy (TEM) after

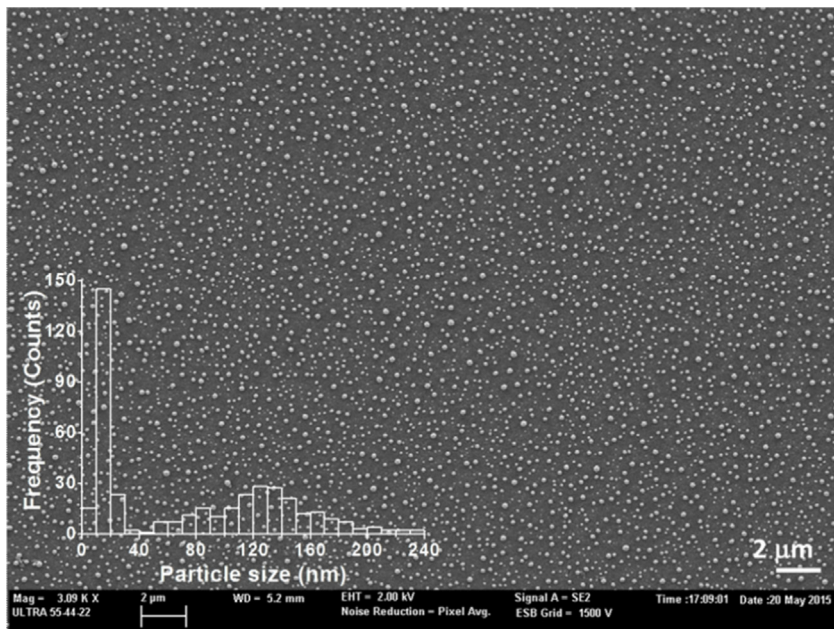


**Fig. 1.** Large field FESEM image of an efficient  $\overline{\text{Cu}_2\text{O}}/\text{fl-G}$  film two days after preparation showing the homogeneous distribution of  $\overline{\text{Cu}_2\text{O}}$  nanoplatelets on  $\text{fl-G}$ . The nanoplatelet size distribution histogram is presented as inset and shows a bimodal distribution with more abundant small size nanoplatelets. At the magnification presented only large particles can be observed.

removal of the quartz substrate. Besides XRD, direct evidence of preferential morphology and facet orientation of  $\text{Cu}_2\text{O}$  particles in  $\overline{\text{Cu}_2\text{O}}/\text{fl-G}$  films was also determined by TEM. In the case of  $\overline{\text{Cu}_2\text{O}}/\text{fl-G}$  films on quartz, TEM imaging required the prior detachment of  $\overline{\text{Cu}_2\text{O}}/\text{fl-G}$  from the quartz substrate with the minimal alteration of the orientation of the particles. This was performed by consecutive careful mechanical polishing of quartz up to 100 nm thickness, followed dimpling grinding and final argon ion milling until complete removal of quartz. The resulting self-standing  $\overline{\text{Cu}_2\text{O}}/\text{fl-G}$  film detached from quartz was introduced directly in the TEM chamber without deposition on a holey copper grid. Preferential facet orientation of  $\text{Cu}_2\text{O}$  nanoplatelets was deduced from comparison of the TEM image with that of the image presenting only those  $\text{Cu}_2\text{O}$  nanoplatelets exhibiting the electron diffraction pattern corresponding to (2.0.0) orientation.

XP spectra were measured on a SPECS spectrometer equipped with a Phoibos 150 9MCD detector using a non-monochromatic X-ray source (Al and Mg) operating at 200 W. The samples were evacuated in the prechamber of the spectrometer at  $1 \cdot 10^{-9}$  mbar. The measured intensity ratios of the components were obtained from the area of the corresponding peaks after nonlinear Shirley-type background subtraction and corrected by the transition function of the spectrometer.

Atomic force microscopy (AFM) measurements were conducted in the contact mode in air at ambient temperature using a Veeco AFM apparatus. It should be noted that AFM were not measured in a clean room and, therefore, films on quartz substrates may contain dust that will be detectable by these techniques.

Transient absorption (TAS) experiments were recorded using a home-built system as reported before [30]. The samples were excited with a Nd:YAD laser at 532 nm and 1 Hz.

### 2.3. Photocatalytic measurements

The  $\overline{\text{Cu}_2\text{O}}/\text{fl-G}$  films supported on quartz or any other photocatalyst were introduced in a sealed orthogonal photoreactor ( $20 \times 10 \times 4 \text{ cm}^3$ ) of aluminium body and a top quartz window.

Ar-purged water was spread on top of the  $\overline{\text{Cu}_2\text{O}}/\text{fl-G}$  film until complete film coverage. The  $\text{H}_2$  evolution tests were determined by connecting directly the photoreactor to an Agilent 490 Micro GC (Molsieve 5A column with Ar as carrier gas). The light source was a 300 W Xe lamp. The lamp was located at 13 cm distance from the films, achieving an irradiance of  $160 \text{ mW cm}^{-2}$  on the films surface. The temperature and pressure inside the reactor was controlled through a thermocouple and a manometer, respectively. The temperature of the system never overcomes 50 °C, apart from the case of the temperature-production dependence experiments. The photocatalytic activity of each sample was evaluated at least in three independent experiments, without observing significant differences among the various tests.

## 3. Results and discussion

### 3.1. Photocatalyst characterization

Oriented  $\overline{\text{Cu}_2\text{O}}/\text{fl-G}$  films were prepared as reported by pyrolysis at 900 °C under inert atmosphere of a  $\text{Cu}^{2+}$ -chitosan film of nanometric thickness on quartz and spontaneous oxidation by exposure to the ambient atmosphere, except that for the present application high Cu loading was found beneficial [33]. The process forms initially metallic Cu particles that are subsequently converted into  $\text{Cu}_2\text{O}$ . Characterization by ICP-OES elemental analysis showed that the Cu content of the most efficient  $\overline{\text{Cu}_2\text{O}}/\text{fl-G}$  films prepared was  $4.75 \mu\text{g/cm}^2$ . As it can be observed in the FESEM images of Fig. 1,  $\text{Cu}_2\text{O}$  nanoplatelets appeared homogeneously distributed on the few-layers G support. From these images at different magnifications a bimodal size distribution was observed. The average size of each type of nanoplatelet was determined by measuring a statistically relevant number of particles. The smallest ones exhibit a size distribution between 5 and 20 nm with an average about 8 nm. The biggest nanoplatelets have a broader distribution between 40 and 200 nm and an average of 130 nm. Moreover, AFM images confirm the uniform nanoplatelet distribution over the few-layers G sheet (20 nm thickness) and the presence of two main size groups with

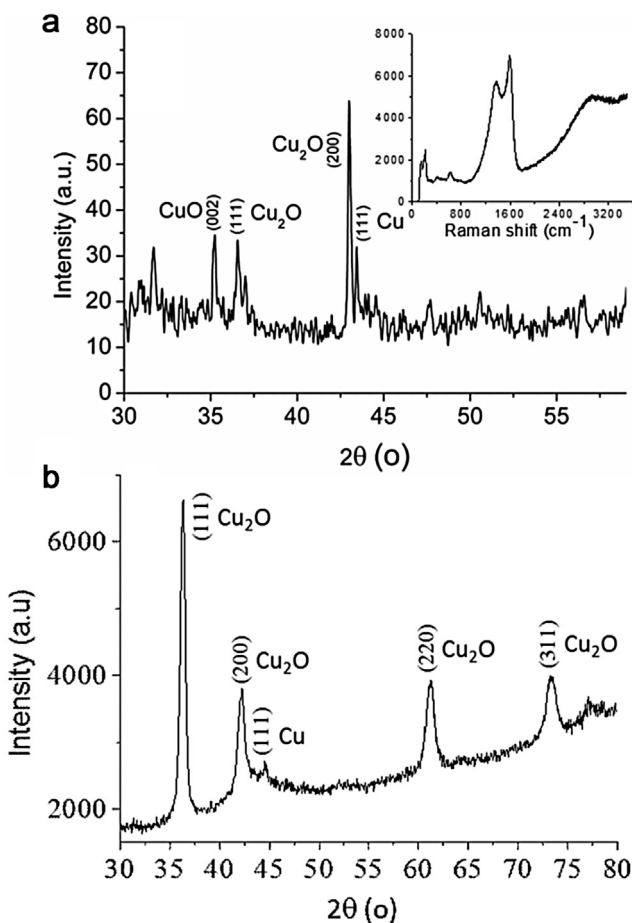


**Fig. 2.** (a) XRD pattern recorded for the  $\overline{\text{Cu}_2\text{O}}/\text{fl-G}$  film ( $4.75 \mu\text{g}/\text{cm}^2$ ) two days after its preparation in which the corresponding peaks have been indexed. The inset shows the corresponding Raman spectrum of the sample recorded with  $512 \text{ nm}$  excitation. Note that the peaks appearing in the Raman spectrum at wavenumbers below  $800 \text{ cm}^{-1}$  are attributable to  $\text{Cu}_2\text{O}$ ; (b) XRD of unoriented  $\text{Cu}_2\text{O}/\text{fl-G}$  film that agrees well with reported patterns for conventional  $\text{Cu}_2\text{O}$  samples. Note that the area of the  $(1.1.1)$  peak is 2.5 fold higher than that of  $(2.0.0)$  for unoriented  $\text{Cu}_2\text{O}/\text{fl-G}$ , while in the case of  $\overline{\text{Cu}_2\text{O}}/\text{fl-G}$  film the  $(2.0.0)$  peak is about 3 times larger than that corresponding to the  $(1.1.1)$  facet.

a uniform height of about 20–30 nm (see Fig. S1 in Supplementary information). The origin of this bimodal distribution is probably related to the preparation procedure of  $\overline{\text{Cu}_2\text{O}}/\text{fl-G}$  films and the mechanism in which Cu nanoplatelets are generated and grow during the pyrolysis at  $900^\circ\text{C}$  by agglomeration of small melted Cu nanodrops on G. Thus, large  $\text{Cu}_2\text{O}$  nanoplatelets are surrounded by a circular zone in where small  $\text{Cu}_2\text{O}$  particles are located having a central larger particle.

Raman spectroscopy of  $\overline{\text{Cu}_2\text{O}}/\text{fl-G}$  films showed the corresponding D and G bands expected for graphene sheets with defects due to the presence of residual oxygenated functional groups remaining from the initial polysaccharide precursor (see insert in Fig. 2). In addition, the low frequency region of the Raman spectra shows the characteristic vibration bands of  $\text{Cu}_2\text{O}$  at 635, 436 and  $218 \text{ cm}^{-1}$ , providing information of the oxidation state of the Cu species (a magnified image of this region can be seen in Fig. S2 in supplementary Information). While metallic Cu(0) is silent in Raman spectroscopy and it does not exhibit any specific absorption peak, CuO exhibits characteristic vibration bands at 615, 330 and  $280 \text{ cm}^{-1}$  that in the present case of  $\overline{\text{Cu}_2\text{O}}/\text{fl-G}$  films were below the detection limit [31,32]. This agrees with previous observations that

G stabilizes preferentially Cu(I) oxidation state over Cu(II) that are formed by spontaneous oxidation of metallic Cu particles [33,34].

In the related precedent, the low concentration of Cu present on fl-G ( $2.5 \text{ ng}/\text{cm}^2$ ) precluded the observation of any XRD pattern characteristic of Cu species. In the present case, the much higher  $\text{Cu}_2\text{O}$  loading has allowed us recording a XRD of  $\overline{\text{Cu}_2\text{O}}/\text{fl-G}$  films ( $4.75 \mu\text{g}/\text{cm}^2$ ). Fig. 2 presents the XRD pattern of a  $\overline{\text{Cu}_2\text{O}}/\text{fl-G}$  film two days after its preparation. For the sake of comparison Fig. 2 also presents the XRD of an unoriented  $\text{Cu}_2\text{O}/\text{fl-G}$  film, whose XRD agrees well with the conventional XRD pattern expected for  $\text{Cu}_2\text{O}$ . Unoriented  $\text{Cu}_2\text{O}$  NPs were synthesized by ambient oxidation of Cu NPs obtained from the polyol method and supported on fl-G (see Experimental section). On one hand, XRD of the  $\overline{\text{Cu}_2\text{O}}/\text{fl-G}$  film confirms the presence of  $\text{Cu}_2\text{O}$  as predominant species over metallic Cu or CuO. On the other hand, XRD also proves the preferential (2.0.0) facet orientation of  $\text{Cu}_2\text{O}$  nanoplatelets based on the relative higher intensity of the corresponding peak over the (1.1.1) and the rest of XRD peaks.

Besides XRD, prevalence of  $\text{Cu}_2\text{O}$  over other oxidation states of Cu and preferential orientation of  $\text{Cu}_2\text{O}$  nanoplatelets in  $\overline{\text{Cu}_2\text{O}}/\text{fl-G}$  films was also confirmed by electron microscopy. Fig. 3a and b shows a comparison of the FESEM image with that provided by electron backscattering diffraction of the same region. The coincidence between the two images indicates that most of the nanoplatelets in this  $\overline{\text{Cu}_2\text{O}}/\text{fl-G}$  film correspond to  $\text{Cu}_2\text{O}$ . Preferential 2.0.0 facet orientation of  $\text{Cu}_2\text{O}$  nanoplatelets was assessed by TEM imaging after removing the quartz substrate from the  $\overline{\text{Cu}_2\text{O}}/\text{fl-G}$  film by a combination of mechanical polishing, dimpling grinding and Ar ion sputtering to avoid alteration of the orientation of  $\text{Cu}_2\text{O}$  nanoplatelets. The self-standing  $\overline{\text{Cu}_2\text{O}}/\text{fl-G}$  films could be observed by transmission techniques. Comparison of the TEM image with that corresponding to the fraction of those particles showing 2.0.0 facet orientation is provided in Fig. 3 panels c and d. Using ImageJ software, it was estimated that about 85% of the  $\text{Cu}_2\text{O}$  nanoplatelets observed in TEM have 2.0.0 facet orientation.

Fig. 4 shows the high resolution XPS spectra, C1s and Cu2p peaks and the best deconvolution to individual components. As it can be seen in this Figure, XP spectra show the presence of Cu(I) (933 eV peak) and Cu(II) (935 eV peak) on the outermost layers of the oriented  $\overline{\text{Cu}_2\text{O}}/\text{fl-G}$  film. Since Cu(II) was not detected neither in Raman spectroscopy nor in FESEM imaging, it can be concluded that the presence of this oxidation state has to be limited just to a shallow outermost layer of  $\text{Cu}_2\text{O}$  nanoplatelets of less than a few nm. In addition, Auger peak reveals that the absence of Cu(0) on the external layers of the nanoplatelets (see Fig. S3). C1s peak in XPS showed narrow 284.5 eV peak corresponding to graphitic C-C and two minor components (<5 atom%) attributable to C atoms bonded to an O and/or a N atoms. The presence of N atoms on the graphene resulting from the pyrolysis of chitosan has been previously reported [35]. Surprisingly, although in previous reports the presence of N atoms in  $\overline{\text{Cu}_2\text{O}}/\text{fl-G}$  films was not observed, in the present case N atoms (about 0.8%) have been detected. Overall all the available characterization data are in agreement with those recently reported for  $\overline{\text{Cu}_2\text{O}}/\text{fl-G}$  films obtained using the same procedure, indicating the predominant presence of (2.0.0) oriented  $\text{Cu}_2\text{O}$  nanoplatelets strongly grafted on few layers graphene [29].

### 3.2. Photocatalytic measurements

The purpose of the present study was to test the photocatalytic activity of  $\overline{\text{Cu}_2\text{O}}/\text{fl-G}$  films on quartz for overall water splitting. Towards this goal, a film of  $\overline{\text{Cu}_2\text{O}}/\text{fl-G}$  ( $5.8 \mu\text{g} (\text{Cu} + \text{G})/\text{cm}^2$ ) was

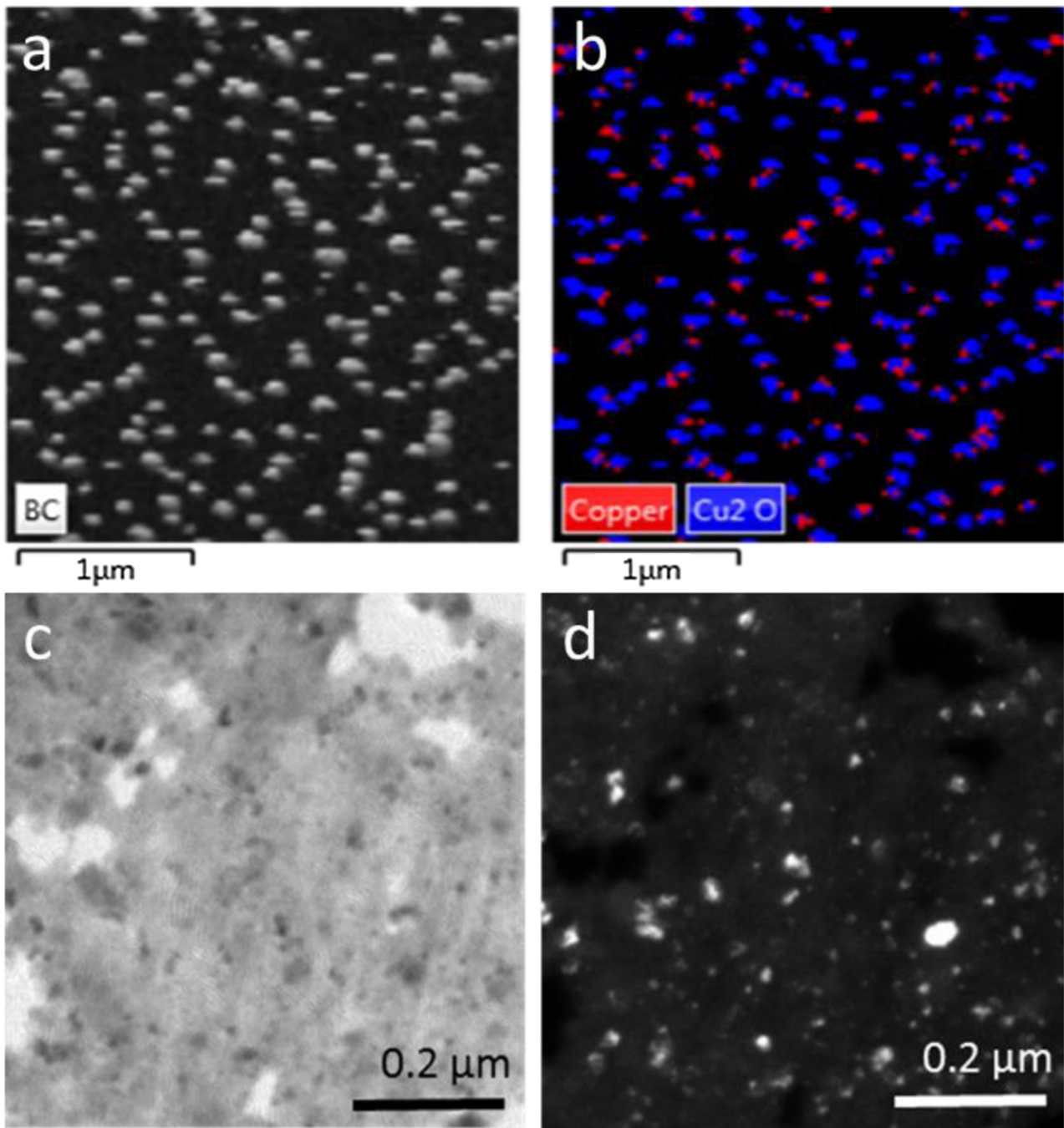


**Fig. 3.** a: FESEM image of  $\overline{\text{Cu}_2\text{O}/\text{fl-G}}$  film two days after preparation. b: Image of the same area as a, but obtained by overlapping the particles having the electron diffraction corresponding to Cu(I) (blue) and Cu(0) (red). c: TEM image of self-supported  $\overline{\text{Cu}_2\text{O}/\text{fl-G}}$  film after removal of quartz substrate. The holes of the film are due to the process of mechanical removal of quartz. d: Image of the same area as c, but presenting only those  $\text{Cu}_2\text{O}$  particles that have the characteristic electron diffraction of the 2.0.0 facet. (For interpretation of the references to color in this figure legend, the reader is referred to the web version of this article.)

placed in a closed reactor under Ar atmosphere and previously Ar-purged water drops were put on the film. The  $\overline{\text{Cu}_2\text{O}/\text{fl-G}}$  film wetted with the water drops on top of it was irradiated at ambient temperature without any stirring with UV-vis light with a 300W Xe lamp (160 mW/cm<sup>2</sup>) at 13 cm distance (see Scheme 1). It is worth to note that after 24 h irradiation some liquid water was still visually remaining on top of the films. The temperature of the  $\overline{\text{Cu}_2\text{O}/\text{fl-G}}$  film never overcomes 50 °C in most of the experiments. However, to determine the influence of the temperature on the photocatalytic overall water splitting an additional experiment was carried

out at 75 °C, by heating the stainless steel photoreactor with a hot plate and controlling the internal temperature with a thermocouple. At this temperature, a decrease in the H<sub>2</sub> production rate of approximately 50% was observed (9.2 mmol/g<sub>Cu+G</sub> h) compared with non-heated photocatalytic experiments. This behavior is not surprising since electron/hole recombination rates in semiconductors usually increase with temperature, and therefore the yield of hydrogen production should be diminished when temperature increases due to a more efficient electron/hole recombination. It is also important to indicate that mechanocatalytic H<sub>2</sub> generation previously reported for Cu<sub>2</sub>O cannot contribute in the present case

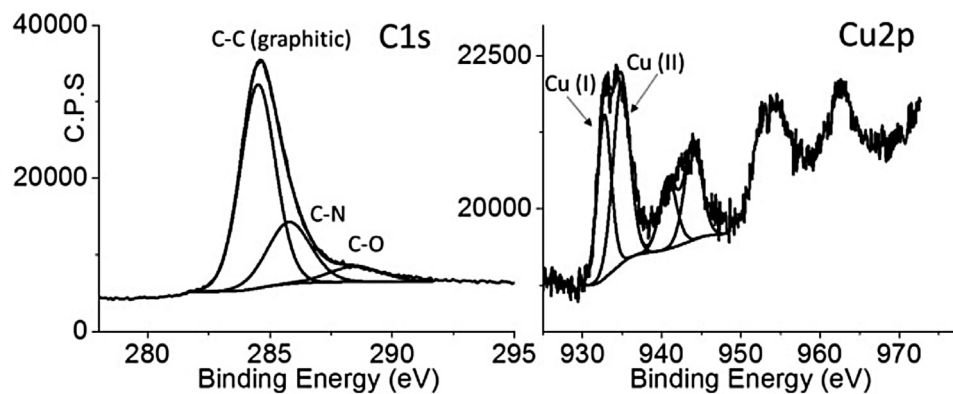


**Fig. 4.** XPS recorded for a  $\overline{\text{Cu}_2\text{O}}/\text{fl-G}$  film ( $4.75 \mu\text{g Cu cm}^{-2}$ ) showing the experimental C1s (a) and the Cu2p (b) peaks and their best deconvolution to individual components, as indicated in the panels.

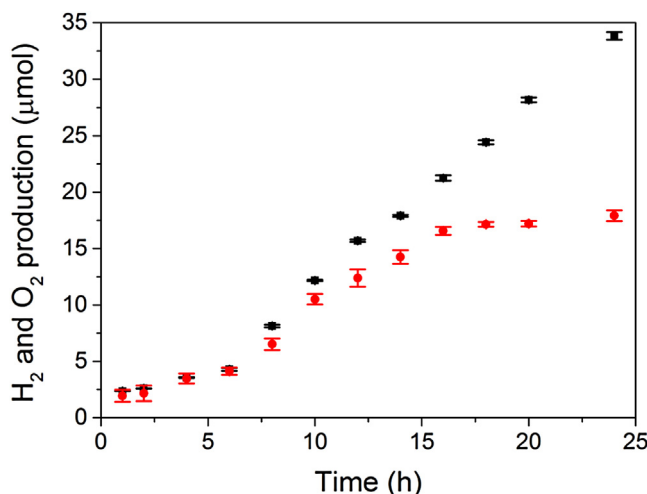


**Fig. 5.** Raw  $\text{H}_2$  (black squares) and  $\text{O}_2$  (red dots) production from  $\overline{\text{Cu}_2\text{O}}/\text{fl-G}$  film ( $12.5 \text{ cm}^2$ ) as function of time upon UV-vis light irradiation from a 300 W Xe lamp. The productivity data correspond to  $19.5 \text{ mmol/g}_{\text{Cu+G}} \text{ h}$ . (For interpretation of the references to color in this figure legend, the reader is referred to the web version of this article.)

to any  $\text{H}_2$  generation due to the static conditions and the absence of any type of stirring [36,37]. No gas evolution was observed in the dark with the lamp on but covering the photoreactor with aluminium foil. In contrast, generation of  $\text{H}_2$  and  $\text{O}_2$  was observed in all the experiments upon illumination of  $\overline{\text{Cu}_2\text{O}}/\text{fl-G}$  in the absence of any sacrificial electron donor. The temporal evolution of the photocatalytic  $\text{H}_2$  and  $\text{O}_2$  production is shown in Fig. 5. A productivity value of  $19.5 \text{ mmol/g}_{\text{Cu+G}} \text{ h}$  and a turnover number of 68 mol  $\text{H}_2/\text{mol Cu}$  was reached at 24 h.

For comparison, an aqueous dispersion of  $\text{Cu}_2\text{O}$  NPs without any preferential orientation supported in fl-G powder ( $\overline{\text{Cu}_2\text{O}}/\text{fl-G}$ ) was submitted to identical light irradiation. Unoriented  $\text{Cu}_2\text{O}$  NPs (7 nm average particle size) were synthetized by ambient oxidation of Cu NPs obtained from the polyol method and supported on fl-G (see Experimental section). In addition, commercial  $\text{Cu}_2\text{O}$  NPs stabilized in ethanol (<350 nm particle size) were also used to test their photocatalytic  $\text{H}_2$  evolution from water under UV-vis light. In all cases, the simultaneous generation of  $\text{H}_2$  and  $\text{O}_2$  was observed, as reported in the literature for  $\text{Cu}_2\text{O}$  NPs [22]. The results of  $\text{H}_2$  production using different photocatalysts and conditions are summarized in Table 1 in where the average of three or more independent measurements and the corresponding estimated errors have been indicated.

Control experiments were carried out in the absence of light for which no  $\text{H}_2$  evolution was detected. The use of oriented  $\overline{\text{Cu}_2\text{O}}/\text{fl-G}$  produced 4 orders of magnitude more  $\text{H}_2$  than an active sample of unoriented  $\text{Cu}_2\text{O}$  NPs supported on fl-G ( $\text{Cu+G}$  content 30 mg,  $\text{H}_2$  production  $0.0046 \text{ mmol H}_2/\text{g}_{\text{Cu+G}} \text{ h}$ ). Note that if unoriented  $\text{Cu}_2\text{O}/\text{fl-G}$  having similar Cu content as  $\overline{\text{Cu}_2\text{O}}/\text{fl-G}$  (0.022 mg Cu, see Table 1) is irradiated, no  $\text{H}_2$  evolution is observed under the same conditions, probably due to the very low photocatalytic activity of this sample of unoriented  $\text{Cu}_2\text{O}/\text{fl-G}$  film with a minute  $\text{Cu}_2\text{O}$  amount. This contrasting activity is indicating that the  $\overline{\text{Cu}_2\text{O}}/\text{fl-G}$  samples prepared by pyrolysis, exhibiting a strong  $\overline{\text{Cu}_2\text{O}}\text{-G}$  grafting and having preferential (2.0.0) orientation in the  $\overline{\text{Cu}_2\text{O}}/\text{fl-G}$ , are catalytically more active in the photocatalytic  $\text{H}_2$  evolution than samples prepared by adsorption on preformed G that do not exhibit any preferential orientation. Moreover, in a related precedent, a superior  $\text{H}_2$  production was demonstrated when rhombic dodecahedra  $\text{Cu}_2\text{O}$  NPs with (110) facets were used instead of  $\text{Cu}_2\text{O}$  cubes with (100) facets or octahedral with (111) facets [24], indicating that some specific orientations might present improved photocatalytic activity than others. Unfortunately, the synthetic procedure employed in this manuscript does not allow us controlling selectively at will the growth of different facets of  $\text{Cu}_2\text{O}$  on G and, therefore, it still remains to be determine if other facets could exhibit an even higher photocatalytic activity for  $\text{H}_2$  evolution. However, what our results establish is that the pyrolytic preparation procedure leading to the preferential orientation of one of the  $\text{Cu}_2\text{O}$  facets renders a material that is several orders of magnitude more efficient for the photocatalytic overall water splitting compared with unoriented samples.

It is very likely that the strong  $\overline{\text{Cu}_2\text{O}}\text{-G}$  interaction favors the interfacial electron transfer between the components of the photocatalytic system, rendering charge separation more efficient. This electron migration from a semiconductor to G is widely accepted as the reason why G as additive in a few weight percents increases the photocatalytic activity of  $\text{TiO}_2$  and other semiconductors [25,38]. In the present case, the one-step pyrolysis procedure for preparation of  $\overline{\text{Cu}_2\text{O}}/\text{fl-G}$  should be not only responsible for preferential 2.0.0 facet orientation of resulting  $\text{Cu}_2\text{O}$ , but also for strong grafting of  $\overline{\text{Cu}_2\text{O}}$  nanoplatelets on fl-G.

In addition, control experiments confirmed that the use of commercial  $\text{Cu}_2\text{O}$  NPs in sufficient amount (2.665 mg) without graphene results in a weak photocatalytic activity, while fl-G without  $\text{Cu}_2\text{O}$  NPs did not show any catalytic activity. This is indicating that the only catalytically active site is the  $\text{Cu}_2\text{O}$  NPs, and G is acting firstly as support of the NPs, secondly as co-catalyst and also

**Table 1**

$\text{H}_2$  production from water in the absence of sacrificial electron donors using oriented (entries 1–3) and non-oriented  $\text{Cu}_2\text{O}$  NPs (4 and 5) supported on few-layers G and  $\text{Cu}_2\text{O}$  NPs (entries 6 and 7) upon UV-vis light irradiation from a 300 W Xe lamp.

Photocatalyst	Cu + G amount (mg) <sup>a</sup>	Reaction time (h)	Average $\text{H}_2$ production (mmol/g h) <sup>b</sup>
$\text{Cu}_2\text{O}/\text{fl-G}$	0.072	24	$19.5 \pm 0.3$
$\text{Cu}_2\text{O}/\text{fl-G}^c$	0.099	24	$3.70 \pm 0.01$
$\text{Cu}_2\text{O}/\text{fl-G}$	30	17	$0.0046 \pm 0.0001$
$\text{Cu}_2\text{O}/\text{fl-G}$	0.022	20	— <sup>d</sup>
$\text{Cu}_2\text{O}$ NPs	2.665	20	$0.047 \pm 0.007$
$\text{Cu}_2\text{O}$ NPs	0.050	20	— <sup>d</sup>
$\text{Cu}_2\text{O}$ NPs (0.3–0.5 $\mu\text{m}$ )	500	1900	0.004 <sup>e</sup>
Ru <sub>2</sub> O decorated $\text{Cu}_2\text{O}$ NPs	500	400	0.0008 <sup>f</sup>
$\text{Cu}_2\text{O}$ NPs (100–300 nm)	20	120	0.0013 <sup>g</sup>

<sup>a</sup> For the hydrogen production the films, total amounts has taken into account since G could have photocatalytic activity.

<sup>b</sup> Formation of  $\text{O}_2$  in quasi stoichiometric amounts was observed.

<sup>c</sup> Irradiated only with visible light using a cut-off filter of 405 nm.

<sup>d</sup> No  $\text{H}_2$  was detected.

<sup>e</sup> Data reported in Ref. [22], the photocatalytic experiment was carried out in a 200  $\text{cm}^3$  pyrex cell under a 300 W Xe lamp ( $\lambda > 460$  nm).

<sup>f</sup> Data obtained from Ref. [39], the photocatalytic reaction was performed irradiating a pyrex cell with a 300 W Xe lamp ( $\lambda > 450$  nm).

<sup>g</sup> Data obtained from Ref. [40], the photocatalysis was carried out in a 20  $\text{cm}^3$  glass vessel with a 150 W halogen lamp (irradiation 350 mW/cm<sup>2</sup>).

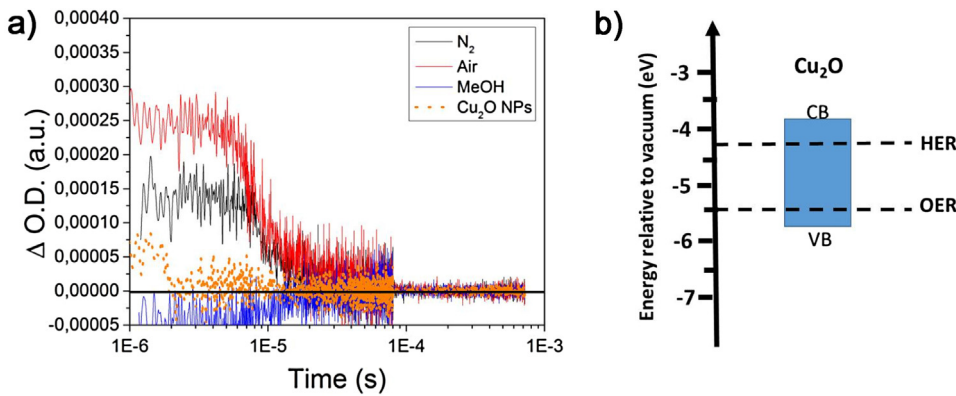


**Fig. 6.** (a) Transient absorption kinetics of a  $\text{Cu}_2\text{O}/\text{fl-G}$  film measured under  $\text{N}_2$  (black), air (red) and MeOH (blue) atmospheres and  $\text{Cu}_2\text{O}$  NPs suspension (orange). The excitation wavelength was 532 nm, and the monitoring wavelength 600 nm. (b) Energy band alignment of  $\text{Cu}_2\text{O}$  respect oxygen and hydrogen evolution reactions. (For interpretation of the references to color in this figure legend, the reader is referred to the web version of this article.)

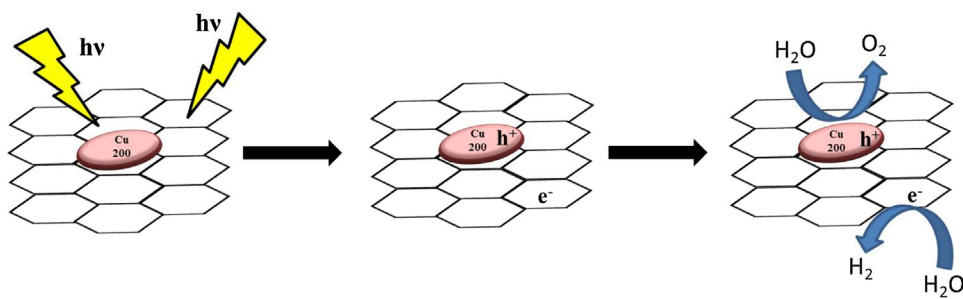
as templating agent favoring the preferential (200) facets orientation. It is worth noticing that commercial  $\text{Cu}_2\text{O}$  NPs has presented higher activity than unoriented  $\text{Cu}_2\text{O}/\text{fl-G}$ , but still orders of magnitude lower than that of  $\text{Cu}_2\text{O}/\text{fl-G}$ . It should be commented that the possibility that some residual ethanol, favoring  $\text{H}_2$  evolution in commercial  $\text{Cu}_2\text{O}$  NPs by acting as sacrificial electron donor cannot be totally excluded in this case, since the commercial  $\text{Cu}_2\text{O}$  nanoparticles are stabilized in ethanol to avoid their oxidation.

It should be also commented that when similar amount of  $\text{Cu}_2\text{O}$  (50  $\mu\text{g}$  Cu, see Table 1) as that present in  $\text{Cu}_2\text{O}/\text{fl-G}$  films was used as photocatalyst for comparison, no evidence of photocatalytic  $\text{H}_2$  generation was obtained and, for this reason, it was necessary to use higher amounts (2.665 mg) to observe  $\text{H}_2$  evolution.

The extraordinary efficiency of  $\text{Cu}_2\text{O}/\text{fl-G}$  film as photocatalyst compared to its congeners has to derive in part from the activity of fl-G as co-catalyst. To obtain some evidence of the photochemical generation of the state of charge separation upon irradiation of the  $\text{Cu}_2\text{O}/\text{fl-G}$  film, transient absorption measurements of the film were performed using a pulsed ns laser system. Thus, monitoring at 600 nm a transient signal could be observed for the  $\text{Cu}_2\text{O}/\text{fl-G}$  films upon 532 nm excitation under nitrogen. The intensity of the transient signal immediately after the laser pulse increased under air atmosphere. When excitation was carried out in the presence of methanol as electron donor disappearance of the transient signal was observed. Fig. 6(a) shows the temporal profiles of the transient

signal monitored at 600 nm recorded for  $\text{Cu}_2\text{O}/\text{fl-G}$  film under the various conditions. These results can be interpreted considering that the 600 nm signal is mostly due to positive holes reaching the microsecond timescale generated on  $\text{Cu}_2\text{O}$  upon photoexcitation, formation of the charge separation state and subsequent electron migration to fl-G. If this is the case, then the presence of  $\text{O}_2$  should increase its initial intensity in the microsecond time scale as consequence of the lesser extent of prompt charge recombination of the hole with electrons, due to their trapping by  $\text{O}_2$ . In contrast, the presence of  $\text{CH}_3\text{OH}$ , a known electron donor, will make the signal of positive holes disappear completely. The lifetimes of these holes in  $\text{Cu}_2\text{O}/\text{fl-G}$  film under  $\text{N}_2$  and  $\text{O}_2$  were estimated from the fitting of the signal to a first-order kinetics as  $\tau_{\text{N}2} = 12.5 \mu\text{s}$  and  $\tau_{\text{O}2} = 11.3 \mu\text{s}$ , respectively. Moreover, a control experiment submitting a suspension of commercial  $\text{Cu}_2\text{O}$  NPs in acetonitrile under air to laser excitation in the same conditions did not allow detecting any transient signal, indicating that G is effectively enhancing the lifetime of charge separation in  $\text{Cu}_2\text{O}/\text{fl-G}$  films.

In view of the previous data, we could establish that the oxygen evolution reaction would take place fundamentally in the  $\text{Cu}_2\text{O}$  nanoplatelets after light excitation. Moreover, as it has been previously reported the  $\text{Cu}_2\text{O}$  valence band position would be enough oxidant to perform  $\text{H}_2\text{O}$  oxidation as can be observed in Fig. 6(b) [41]. Considering that the valence band energy of G has been reported as 5.94 V relative to the vacuum [42], the most likely



**Scheme 2.** Illustration of the role of fl-G enhancing the efficiency of charge separation and the overall photocatalytic efficiency of  $\overline{\text{Cu}_2\text{O}}/\text{fl-G}$ .

mechanism to explain the remarkable photocatalytic activity is illustrated in **Scheme 2**.

For  $\overline{\text{Cu}_2\text{O}}/\text{fl-G}$ , the  $\text{H}_2$  and  $\text{O}_2$  production was also measured under visible light using a cut-off filter of 405 nm. The  $\text{H}_2$  evolution under visible light was  $3.70 \pm 0.01 \text{ mmol/g}_{\text{Cu+G}} \text{ h}$ , as included in **Table 1**. This value is about 19% of the one obtained with full UV-vis light irradiation, after correcting for the different amount of  $\text{Cu}_2\text{O}$ . This percentage indicates that the  $\overline{\text{Cu}_2\text{O}}/\text{fl-G}$  films are also notably active in the visible part of the spectrum. This is in accordance with the 2.0 eV bandgap of  $\text{Cu}_2\text{O}$  [21]. However, when using the unfiltered light from the Xe lamp, the UV region still contributes in a larger extent to the overall activity than visible light.

The Cu amount in the reaction was increased by introducing in the reactor  $\overline{\text{Cu}_2\text{O}}/\text{fl-G}$  films ( $7.88 \mu\text{g}_{\text{Cu+G}}/\text{cm}^2$ ) with larger surface ( $4.8$  and  $16 \text{ cm}^2$ ) in order to elucidate how the photocatalytic overall water splitting was affected by increasing the irradiation area and amount of oriented  $\text{Cu}_2\text{O}$  nanoplatelets. The photocatalytic  $\text{H}_2$  evolution increased linearly with the Cu amount present in the photoreactor as it is presented in Fig. S4 in the Supplementary information. In spite of the small amount of Cu in the G films (in the sub milligram scale), as soon as the Cu mass was increased, the  $\text{H}_2$  and  $\text{O}_2$  production increases as well.

### 3.3. Photocatalyst stability

Besides the improved  $\text{H}_2$  and  $\text{O}_2$  production due to the preferential orientation of the  $\overline{\text{Cu}_2\text{O}}$  nanoplatelets, the use of fl-G as support produced also an enhanced stability when compared with non-supported  $\text{Cu}_2\text{O}$  NPs, which are well-known to rapidly oxidize to  $\text{CuO}$  under photocatalytic conditions [24]. In this regard, a  $\overline{\text{Cu}_2\text{O}}/\text{fl-G}$  film was placed in a crucible filled of Ar-purged water, and the reaction was followed for six days (Fig. 7). As can be observed the photocatalyst still retains approximately about 50% of the activity even after 6 days under continuous irradiation. FESEM images of a six days used  $\overline{\text{Cu}_2\text{O}}/\text{fl-G}$  film showed no alterations in the particle size distribution, remaining the bimodal distribution as that shown in the inset of Fig. 8, excluding any particle growth as the origin of the deactivation. However, nanoplatelets morphology was affected after six days reaction and as can be observed in Fig. 8a the  $\text{Cu}_2\text{O}$  particles present a rough surface with an irregular shape. In order to investigate the origin of the changes in  $\text{Cu}_2\text{O}$  morphology, C1s and Cu2p XPS spectra of a  $\overline{\text{Cu}_2\text{O}}/\text{fl-G}$  film after 6 days reaction were recorded (Fig. 8b). Although the C1s XPS spectrum did not present notable differences, the relative intensities of Cu(I) (933 eV) and Cu(II) (935 eV) peaks varied from the initial spectra presented in Fig. 4. In this case, after six days reaction, the relative intensity of Cu(I) peak decreased respect the Cu(II) peak, indicating that a percentage of Cu(I) has evolved to Cu(II) during the six days reaction time. Thus, the most likely cause of deactivation is the partial transformation of  $\text{Cu}_2\text{O}$  into  $\text{CuO}$ , as it has been reported in the

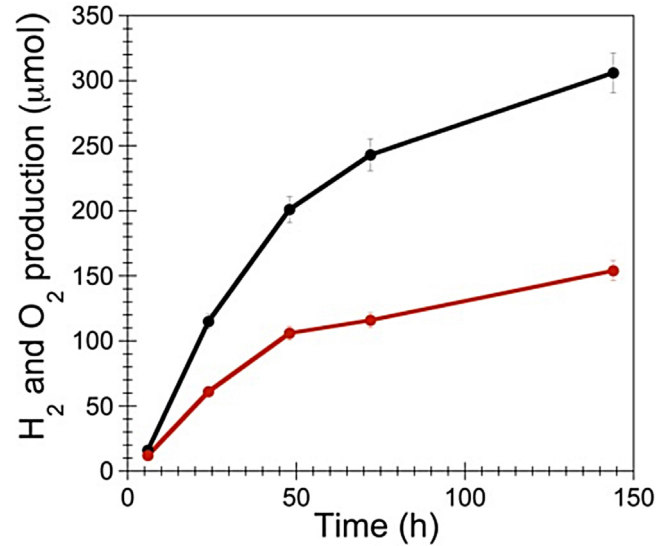


**Fig. 7.**  $\text{H}_2$  and  $\text{O}_2$  production from a  $\overline{\text{Cu}_2\text{O}}/\text{fl-G}$  film containing  $0.099 \text{ mg}$  of  $\text{Cu+G}$  upon UV-vis light irradiation from  $300 \text{ W}$  Xe lamp for six days.

literature for unsupported particles [24,43]. In any case, Fig. 7 indicates a considerable increase in the stability of the  $\text{Cu}_2\text{O}$  supported on fl-G under reaction conditions respect the non-supported  $\text{Cu}_2\text{O}$  NPs and previous investigations [24,43].

### 4. Conclusions

The use of preferentially oriented  $\overline{\text{Cu}_2\text{O}}$  nanoplatelets strongly grafted on few layer G has demonstrated not only three to four orders of magnitude improved  $\text{H}_2$  evolution for the overall water splitting compared the randomly oriented NPs, but also higher stability, exhibiting long-term  $\text{H}_2$  production. This enhanced activity and stability appears to be due to the facet orientation, the strong  $\overline{\text{Cu}_2\text{O}}$ -graphene interaction and the role of G as cocatalyst. Thus, after photon absorption at  $\text{Cu}_2\text{O}$  and occurrence of charge separation, electrons migrate rapidly from  $\text{Cu}_2\text{O}$  to graphene, enhancing in this way the efficiency of charge separation. At this moment, holes should be located at  $\text{Cu}_2\text{O}$  and electrons on graphene. Further studies are directed to show that facet orientation of metal NPs on graphene is a general methodology to render an advanced generation of more efficient photocatalysts for solar fuel production.

### Acknowledgments

Finantial support by the Spanish Ministry of Economy and Competitiveness (Severo Ochoa and CTQ2015-69153-CO2-1-R) and Generalitat Valenciana (Prometeo 2013-019) is gratefully acknowl-

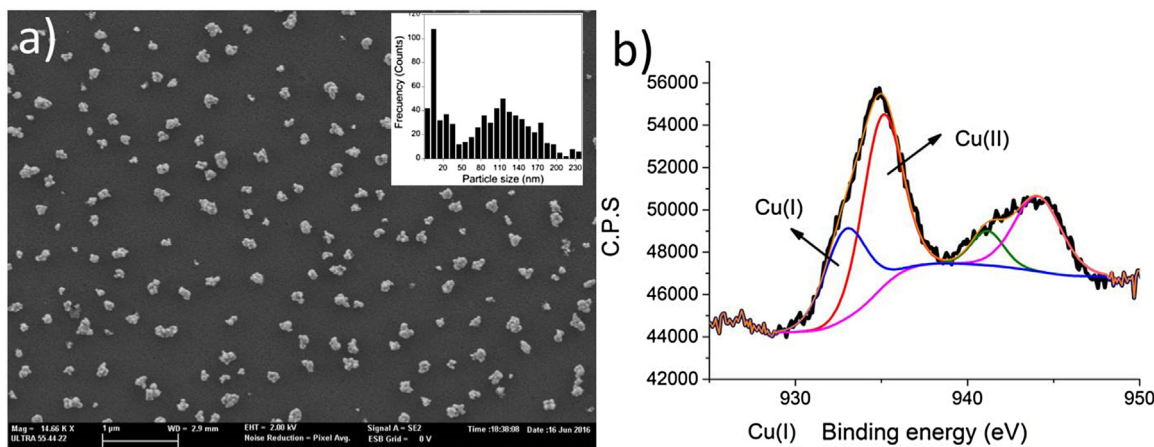


**Fig. 8.** (a) FESEM image from a  $\text{Cu}_2\text{O}/\text{fl-G}$  film ( $4.75 \mu\text{g Cu cm}^{-2}$ ) after six days reaction upon UV-vis light irradiation from 300 W Xe lamp. The inset presents the particle size distribution histogram showing the bimodal distribution. (b) Cu2p XPS spectrum of the same film. Note that no direct quantitative comparison with the Cu2p peak of Fig. 4 can be made due to different acquisition times.

edged. D. M. M. and I. E. A thank to the Technical University of Valencia and the Spanish Ministry of Science for PhD scholarships.

## Appendix A. Supplementary data

Supplementary data associated with this article can be found, in the online version, at <http://dx.doi.org/10.1016/j.apcatb.2016.08.033>.

## References

- [1] J.M. Campelo, D. Luna, R. Luque, J.M. Marinas, A.A. Romero, *ChemSusChem* 2 (2009) 18–45.
- [2] A. Primo, H. Garcia, *New and Future Developments in Catalysis*, in: S.L. Suib (Ed.), Elsevier, Amsterdam, 2013, pp. 425–449.
- [3] H. Ghanbarlou, S. Rowshan Zamir, B. Kazeminasab, M.J. Parnian, *J. Power Sources* 273 (2015) 981–989.
- [4] Y. Wang, Y. Zhao, W. He, J. Yin, Y. Su, *Thin Solid Films* 544 (2013) 88–92.
- [5] Z. Li, J. Liu, Z. Huang, Y. Yang, C. Xia, F. Li, *ACS Catal.* 3 (2013) 839–845.
- [6] Y. Roman-Leshkov, C.J. Barrett, Z.Y. Liu, J.A. Dumesic, *Nature* 447 (2007) 982–985.
- [7] A.S. Arico, P. Bruce, B. Scrosati, J.-M. Tarascon, W. van Schalkwijk, *Nat. Mater.* 4 (2005) 366–377.
- [8] N.J. Divins, I. Angurell, C. Escudero, V. Pérez-Dieste, J. Llorca, *Science* 346 (2014) 620–623.
- [9] C.T. Campbell, *Nat. Chem.* 4 (2012) 597–598.
- [10] J. Albero, H. Garcia, *J. Mol. Catal. A: Chem.* 408 (2015) 296–309.
- [11] C.N.R. Rao, A.K. Sood, K.S. Subrahmanyam, A. Govindaraj, *Angew. Chem. Int. Ed.* 48 (2009) 7752–7777.
- [12] S. Navalon, A. Dhakshinamoorthy, M. Alvaro, H. Garcia, *Coord. Chem. Rev.* (2016).
- [13] E. Yoo, T. Okata, T. Akita, M. Kohyama, J. Nakamura, I. Honma, *Nano Lett.* 9 (2009) 2255–2259.
- [14] B. Das, B. Choudhury, A. Gomathi, A.K. Manna, S.K. Pati, C.N.R. Rao, *ChemPhysChem* 12 (2011) 937–943.
- [15] P. Lazar, S. Zhang, K. Šafářová, Q. Li, J.P. Froning, J. Granatier, P. Hobza, R. Zbořil, F. Besenbacher, M. Dong, M. Otyepka, *ACS Nano* 7 (2013) 1646–1651.
- [16] T. Liao, Z. Sun, C. Sun, S.X. Dou, D.J. Searles, *Sci. Rep.* 4 (2014) 6256.
- [17] W. Zhang, Y. Li, X. Zeng, S. Peng, *Sci. Rep.* 5 (2015) 10589.
- [18] N. Naseri, P. Sangpour, S.H. Mousavi, *RSC Adv.* 4 (2014) 46697–46703.
- [19] J. Yu, L. Qi, M. Jaroniec, *J. Phys. Chem. C* 114 (2010) 13118–13125.
- [20] M. Serra, J. Albero, H. Garcia, *ChemPhysChem* 16 (2015) 1842–1845.
- [21] G. Nagasubramanian, A.S. Gioda, A.J. Bard, *J. Electrochem. Soc.* 128 (1981) 2158–2164.
- [22] M. Hara, T. Kondo, M. Komoda, S. Ikeda, J.N. Kondo, K. Domen, M. Hara, K. Shinohara, A. Tanaka, *Chem. Commun.* (1998) 357–358.
- [23] W.-T. Kung, Y.-H. Pai, Y.-K. Hsu, C.-H. Lin, C.-M. Wang, *Opt. Express* 21 (2013) A221–A228.
- [24] Y. Kwon, A. Soon, H. Han, H. Lee, *J. Mater. Chem. A* 3 (2015) 156–162.
- [25] D. Zhang, D. Wei, Z. Cui, S. Wang, S. Yang, M. Cao, C. Hu, *Phys. Chem. Chem. Phys.* 16 (2014) 25531–25536.
- [26] L.I. Bendavid, E.A. Carter, *J. Phys. Chem. B* 117 (2013) 15750–15760.
- [27] Z. Li, C.V. Ciobanu, J. Hu, J.-P. Palomares-Baez, J.-L. Rodriguez-Lopez, R. Richards, *Phys. Chem. Chem. Phys.* 13 (2011) 2582–2589.
- [28] H. Lee, *RSC Adv.* 4 (2014) 41017–41027.
- [29] A. Primo, I. Esteve-Adell, J.F. Blandez, A. Dhakshinamoorthy, M. Alvaro, N. Candu, S.M. Coman, V.I. Parvulescu, H. Garcia, *Nat. Commun.* 6 (2015).
- [30] E. Palomares, M.V. Martinez-Diaz, S.A. Haque, T. Torres, J.R. Durrant, *Chem. Commun.* (2004) 2112–2113.
- [31] K. Reimann, K. Syassen, *Phys. Rev. B* 39 (1989) 11113–11119.
- [32] B. Balamurugan, I. Aruna, B.R. Mehta, S.M. Shivaprasad, *Phys. Rev. B* 69 (2004) 165419.
- [33] S. Wu, Z. Yin, Q. He, G. Lu, X. Zhou, H. Zhang, *J. Mater. Chem.* 21 (2011) 3467–3470.
- [34] L. Jiang, T. You, P. Yin, Y. Shang, D. Zhang, L. Guo, S. Yang, *Nanoscale* 5 (2013) 2784–2789.
- [35] A. Primo, P. Atienzar, E. Sanchez, J.M. Delgado, H. Garcia, *Chem. Commun.* 48 (2012) 9254–9256.
- [36] S. Ikeda, T. Takata, T. Kondo, G. Hitoki, M. Hara, J.N. Kondo, K. Domen, H. Hosono, H. Kawazoe, A. Tanaka, *Chem. Commun.* (1998) 2185–2186.
- [37] S. Ikeda, T. Takata, M. Komoda, M. Hara, J.N. Kondo, K. Domen, A. Tanaka, H. Hosono, H. Kawazoe, *Phys. Chem. Chem. Phys.* 1 (1999) 4485–4491.
- [38] D.C.B. Alves, R. Silva, D. Voiry, T. Asefa, M. Chhowalla, *Mater. Renew. Sustain. Energy* 4 (2015) 1–7.
- [39] P.C. Ghosh, T. Banerjee, A. Mukherjee, *Energy Procedia* 54 (2014) 221–227.
- [40] S. Kakuta, T. Abe, *Electrochim. Solid State Lett.* 12 (2009) P1–P3.
- [41] A. Martinez-Garcia, V.K. Vendra, S. Sunkara, P. Haldankar, J. Jasinski, M.K. Sunkara, *J. Mater. Chem. A* 1 (2013) 15235–15241.
- [42] D. Mateo, I. Esteve-Adell, J. Albero, J.F.S. Royo, A. Primo, H. Garcia, *Nat. Commun.* 7 (2016).
- [43] A. Paracchino, V. Laporte, K. Sivula, M. Grätzel, E. Thimsen, *Nat. Mater.* 10 (2011) 456–461.